

1 Potential underestimation of ambient brown carbon absorption  
2 based on the methanol extraction method and its impacts on  
3 source analysis

4  
5 Zhenqi Xu<sup>a</sup>, Wei Feng<sup>a</sup>, Yicheng Wang<sup>a</sup>, Haoran Ye<sup>a</sup>, Yuhang Wang<sup>b</sup>, Hong Liao<sup>a</sup>,  
6 Mingjie Xie<sup>a,\*</sup>

7  
8 <sup>a</sup>Collaborative Innovation Center of Atmospheric Environment and Equipment  
9 Technology, Jiangsu Key Laboratory of Atmospheric Environment Monitoring and  
10 Pollution Control, School of Environmental Science and Engineering, Nanjing  
11 University of Information Science & Technology, 219 Ningliu Road, Nanjing 210044,  
12 China

13 <sup>b</sup>School of Earth and Atmospheric Sciences, Georgia Institute of Technology, Atlanta,  
14 GA 30332, United States

15  
16 \*Corresponding to:

17 Mingjie Xie (mingjie.xie@nuist.edu.cn, mingjie.xie@colorado.edu);

18 Mailing address: 219 Ningliu Road, Nanjing, Jiangsu, 210044, China

28 **Abstract**

29       The methanol extraction method was widely applied to isolate organic carbon (OC)  
30 from ambient aerosols, followed by measurements of brown carbon (BrC) absorption.  
31 However, undissolved OC fractions will lead to underestimated BrC absorption. In this  
32 work, water, methanol (MeOH), MeOH/dichloromethane (MeOH/DCM, 1:1, v/v),  
33 MeOH/DCM (1:2, v/v), tetrahydrofuran (THF), and N,N-dimethylformamide (DMF)  
34 were tested for extraction efficiencies of ambient OC, and the light absorption of  
35 individual solvent extracts was determined. Among the five solvents and solvent  
36 mixtures, DMF dissolved the highest fractions of ambient OC (up to ~95%), followed  
37 by MeOH and MeOH/DCM mixtures (< 90%), and the DMF extracts had significant  
38 ( $p < 0.05$ ) higher light absorption than other solvent extracts. This is because the OC  
39 fractions evaporating at higher temperatures ( $> 280^{\circ}\text{C}$ ) are less soluble in MeOH (~80%)  
40 than in DMF (~90%) and contain stronger light-absorbing chromophores. Moreover,  
41 the light absorption of DMF and MeOH extracts of collocated aerosol samples in  
42 Nanjing showed consistent temporal variations in winter when biomass burning  
43 dominated BrC absorption. While the average light absorption of DMF extracts was  
44 more than two times greater than the MeOH extracts in late spring and summer. The  
45 average light absorption coefficient at 365 nm of DMF extracts was 30.7% higher ( $p <$   
46  $0.01$ ) than that of MeOH extracts. Source apportionment results indicated that the  
47 MeOH solubility of BrC associated with biomass burning, lubricating oil combustion,  
48 and coal combustion is similar to their DMF solubility. The BrC linked with unburned  
49 fossil fuels and polymerization processes of aerosol organics was less soluble in MeOH  
50 than in DMF, which was likely the main reason for the large difference in time series  
51 between MeOH and DMF extract absorption. These results highlight the importance of  
52 testing different solvents to investigate the structures and light absorption of BrC,

53 particularly for the low-volatility fraction potentially originating from non-combustion  
54 sources.

55

56

57

58

59

60

61

62

63

64

65

66

67

68

69

70

71

72

73

74

75

76

77

## 78 **1 Introduction**

79 Besides black carbon (BC) and mineral dust, growing evidence shows that organic  
80 carbon (OC) aerosols derived from various combustion sources (e.g., biofuel and fossil  
81 fuel) and secondary processes (e.g., gas-phase oxidation, aqueous and in-cloud  
82 processes) can absorb sunlight at short visible and UV wavelengths (Laskin et al., 2015;  
83 Hems et al., 2021). The radiative forcing (RF) of the light-absorbing organic carbon,  
84 also termed “brown carbon” (BrC), is not well quantified due to the lack of its emission  
85 data, complex secondary formations, and large uncertainties in *in situ* BrC  
86 measurements (Wang et al., 2014; Wang et al., 2018; Saleh, 2020). The imaginary part  
87 of the refractive index ( $k$ ) of BrC is required when modeling its influence on aerosols  
88 direct RF, and is retrieved by the optical closure method combining online monitoring of  
89 aerosol absorption and size distributions with Mie theory calculations (Lack et al., 2012;  
90 Saleh et al., 2013; Saleh et al., 2014). However, several pre-assumptions must be made  
91 on aerosol morphology (spherical Mie model) and mixing states of BC and organic  
92 aerosols (OA), which might introduce large uncertainties in the estimation of  $k$  (Mack  
93 et al., 2010; Xu et al., 2021).

94 To improve the understanding on chemical composition and light-absorbing  
95 properties of BrC chromophores, organic matter (OM) in aerosols was isolated through  
96 solvent extraction using water and/or methanol, followed by filtration and a series of  
97 instrumental analysis (e.g., UV/Vis spectrometer, liquid chromatograph-mass  
98 spectrometer; Chen and Bond, 2010; Liu et al., 2013; Lin et al., 2016). Referring to  
99 existing studies, a larger fraction of the methanol extract absorption comes from water-  
100 insoluble OM containing conjugated structures (Chen and Bond, 2010; Huang et al.,  
101 2020); the light absorption of biomass burning OM is majorly contributed by large  
102 molecules (MW > 500~1000 Da; Di Lorenzo and Young, 2016; Di Lorenzo et al., 2017)

103 and depends on burn conditions (Saleh et al., 2014); polycyclic aromatic hydrocarbons  
104 (PAHs) and nitroaromatic compounds (NACs) are ubiquitous BrC chromophores in the  
105 atmosphere (Huang et al., 2018; Wang et al., 2019), but the identified species only  
106 explain a few percentages (< 10%) of total BrC absorption (Huang et al., 2018; Li et  
107 al., 2020).

108 Methanol can extract > 90% OM from biomass burning (Chen and Bond, 2010;  
109 Xie et al., 2017b), while the extraction efficiency ( $\eta$ , %) decreases to ~80% for ambient  
110 organic aerosols (Xie et al., 2019b; Xie et al., 2022) possibly due to other sources  
111 emitting large hydrophobic molecules and oligomerizations of small molecules during  
112 the aging process (Cheng et al., 2021; Li et al., 2021). The light-absorbing properties  
113 and structures of methanol-insoluble OC (MIOC) are still unknown. By comparing BrC  
114 characterization results of offline and online methods, some studies conclude that the  
115 MIOC dominates BrC absorption in source and ambient aerosols (Bai et al., 2020; Atwi  
116 et al., 2022). However, the online-retrieval and offline-extraction methods are designed  
117 based on different instrumentation and purposes, and the online method depends largely  
118 on presumed and uncertain optical properties of BC (Wang et al., 2014). Even when the  
119 solvent extract absorption is converted to particulate absorption with Mie calculations,  
120 pH and solvent matrix effects, as well as the potential incomplete solubility of BrC in  
121 common solvents, should still be considered before comparing BrC absorption  
122 measured directly in particles versus that derived from solvent extracts. To reveal the  
123 absorption and composition of MIOC, it is necessary to find a new solvent or develop  
124 a new methodology to improve OC extraction efficiency (Shetty et al., 2019).

125 In this work, a series of single solvents and solvent blends were tested for extraction  
126 efficiencies of OC in ambient particulate matter with aerodynamic diameter < 2.5  $\mu\text{m}$   
127 ( $\text{PM}_{2.5}$ ), and the sample extract absorption of each solvent was compared. The solvent

128 or solvent mixture with the highest  $\eta$  value was applied to extract a matrix of collocated  
129 PM<sub>2.5</sub> samples followed by light absorption measurements. In our previous work, the  
130 light absorption of methanol extracts of the same samples was measured, and source  
131 apportionment was performed using organic molecular marker data (Xie et al., 2022).  
132 By comparing with the study results in Xie et al. (2022), this study evaluated potential  
133 underestimation of BrC absorption in methanol and its impacts on BrC source  
134 attributions. These results suggest that different solvents should be used in future  
135 investigations on the absorption, composition, sources, and formation pathways of low-  
136 volatility BrC.

## 137 **2. Methods**

### 138 *2.1 Solvent selection*

139 Five solvents and solvent mixtures including water, methanol (MeOH),  
140 MeOH/dichloromethane (MeOH/DCM, 1:1, v:v), MeOH/DCM (1:2, v:v),  
141 tetrahydrofuran (THF), and N,N-dimethylformamide (DMF) were selected to extract  
142 OC from identical PM<sub>2.5</sub> samples to determine which solvent or solvent mixture has the  
143 highest  $\eta$  value. Water and methanol are the most commonly used solvents to extract  
144 BrC from source or ambient particles. Cheng et al. (2021) found that OC produced  
145 through the combustion of toluene, isooctane, and cyclohexane were more soluble in  
146 DCM than MeOH. Since a major part of BrC absorption is coming from unknown large  
147 molecules (Di Lorenzo and Young, 2016; Di Lorenzo et al., 2017), polar aprotic  
148 solvents THF and DMF were tested due to their high capacity for dissolving large  
149 polymers. Except for water and MeOH, DCM and THF were rarely used to extract OC  
150 for light absorption measurements (Cheng et al., 2021; Moschos et al. 2021), and DMF  
151 has not ever been tested for extracting BrC in literature.

### 152 *2.2 Sampling*

153 **Sampling for solvent test.** To compare OC extraction efficiencies and extract  
154 absorption of the five selected solvents and solvent mixtures, twenty-one ambient PM<sub>2.5</sub>  
155 samples were collected on the rooftop of a seven-story library building in Nanjing  
156 University of Information Science and Technology (NUIST, 32.21°N, 118.71°E).  
157 Details of the sampling site and equipment were provided by Yang et al. (2021). Two  
158 identical mid-volume samplers (Sampler I and II; PM<sub>2.5</sub>-PUF-300, Mingye  
159 Environmental, China) equipped with 2.5 μm cut-point impactors were used for  
160 ambient air sampling during day-time (8:00 a.m.–7:00 p.m.) and night-time (8:00 p.m.–  
161 7:00 a.m. the next day), respectively, in December 2019. After the impactor, PM<sub>2.5</sub> in  
162 the air stream was collected on a pre-baked (550 °C, 4 h) quartz filter (20.3 cm ×12.6  
163 cm, Munktell Filter AB, Sweden) at a flow rate of 300 L min<sup>-1</sup>. PM<sub>2.5</sub> filter and field  
164 blank samples were sealed and stored at –20 °C before chemical analysis. Information  
165 about PM<sub>2.5</sub> samples for the solvent test is provided in Table S1 of supplementary  
166 information.

167 **Ambient sampling for BrC analysis.** Details of the ambient sampling were described  
168 in previous work (Qin et al., 2021; Yang et al., 2021; Xie et al., 2022). Briefly, Sampler  
169 I and II were equipped with two quartz filters in series (quartz behind quartz, QBQ  
170 method; Q<sub>f</sub> and Q<sub>b</sub>) followed by adsorbents. Collocated filter and adsorbent samples  
171 were collected every sixth day during daytime and nighttime from 2018/09/28 to  
172 2019/09/28. Field blank sampling was performed every 10<sup>th</sup> sample to address  
173 contamination. Q<sub>f</sub> samples loaded with PM<sub>2.5</sub> were speciated and extracted for light  
174 absorption measurements. The OC adsorbed on Q<sub>b</sub> and its light absorption were  
175 analyzed to determine positive sampling artifacts. The adsorbents in sampler I [a  
176 polyurethane foam (PUF)/XAD-4 resin/PUF sandwich] and II (a PUF plug) were used  
177 to collect gas-phase nonpolar and polar organic compounds, respectively. The

178 measurement results of gas- and particle-phase organic compounds were provided by  
179 Gou et al. (2021) and Qin et al. (2021).

### 180 *2.3 Solvent test for light absorption and extraction efficiency*

181 An aliquot (~6 cm<sup>2</sup>) of each filter sample was extracted ultrasonically in 10 mL of  
182 each solvent or solvent mixture (HPLC grade) for 30 min (one-time extraction  
183 procedure,  $N = 11$ ; Table S1). After filtration, the light absorbance ( $A_\lambda$ ) of individual  
184 solvent extracts was measured over 200–900 nm using a UV/Vis spectrometer (UV-  
185 1900, Shimadzu Corporation, Japan), and was converted to light absorption coefficient  
186 ( $Abs_\lambda$ , Mm<sup>-1</sup>) by

$$187 \quad Abs_\lambda = (A_\lambda - A_{700}) \times \frac{V_l}{V_a \times L} \ln(10) \quad (1)$$

188 where  $A_{700}$  is subtracted to correct baseline drift,  $V_l$  (m<sup>3</sup>) is the air volume of the  
189 extracted sample,  $L$  (0.01 m) is the optical path length, and  $\ln(10)$  was multiplied to  
190 transform  $Abs_\lambda$  from a common to a natural logarithm (Hecobian et al., 2010). To  
191 understand if multiple extractions could draw out more BrC, a two-time extraction  
192 procedure was applied for another 10 ambient PM<sub>2.5</sub> samples in the same manner (Table  
193 S1). The  $A_\lambda$  of the 1<sup>st</sup> and 2<sup>nd</sup> extractions (10 mL each) was measured separately for  
194  $Abs_\lambda$  calculations.

195 Prior to solvent extractions, the concentrations of OC and EC in each filter sample  
196 were analyzed using a thermal-optical carbon analyzer (DRI, 2001A, Atmoslytic,  
197 United States) following the IMPROVE-A protocol. OC and EC were converted to CO<sub>2</sub>  
198 step by step during two separate heating cycles [OC1 (140°C) – OC2 (280°C) – OC3  
199 (480°C) – OC4 (580°C) in pure He, EC1 (580°C) – EC2 (740°C) – EC3 (840°C) in 98%  
200 He/2% O<sub>2</sub>], and the emitted CO<sub>2</sub> during each heating step was converted to CH<sub>4</sub> and  
201 measured using a flame ionization detector (FID).



202 After extractions, filters extracted by MeOH, MeOH/DCM (1:1), MeOH/DCM  
203 (1:2), and THF were air-dried in a fume hood and analyzed for residual OC (rOC,  $\mu\text{g}$   
204  $\text{m}^{-3}$ ) using the identical method. Filters extracted in water and DMF cannot be air-dried  
205 in the short term due to the low volatility of solvents, and their rOC was measured after  
206 baking at 100 °C for 2 h. The total amount of OC dissolved in water for each sample  
207 was also measured as water-soluble OC (WSOC) by a total organic carbon analyzer  
208 (TOC-L, Shimadzu, Japan; Yang et al., 2021). To examine if the baking process would  
209 influence rOC measurements, the rOC of filters extracted in MeOH, MeOH/DCM  
210 mixtures, and THF were also measured after the baking process and compared to those  
211 determined after air dried. The pyrolytic carbon (PC) was used to correct for sample  
212 charring and was determined when the filter transmittance or reflectance returned to its  
213 initial value during the analysis (Schauer et al., 2003), but the formation of PC is very  
214 scarce when analyzing extracted filters. In this study, solvent-extractable OC (SEOC,  
215  $\mu\text{g m}^{-3}$ ) was determined by the difference in OC1–OC4 between pre- and post-  
216 extraction samples. The extraction efficiency ( $\eta$ , %) of each solvent was expressed as

$$217 \quad \eta = \frac{\text{SEOC}}{\text{OC}} \times 100\% \quad (2)$$

218 Here, SEOC denotes WSOC when the solvent is water. For the ambient samples  
219 extracted twice, rOC was measured only after the two-extraction procedure was  
220 completed.

221 The solution mass absorption efficiency ( $\text{MAE}_\lambda$ ,  $\text{m}^2 \text{g}^{-1} \text{C}$ ) was calculated by  
222 dividing  $\text{Abs}_\lambda$  by the concentration of SEOC

$$223 \quad \text{MAE}_\lambda = \frac{\text{Abs}_\lambda}{\text{SEOC}} \quad (3)$$

224 and the solution absorption Ångström exponent ( $\text{Å}$ ), a parameter showing the  
225 wavelength dependence of solvent extract absorption, was obtained from the regression

226 slope of  $\lg(\text{Abs}_\lambda)$  versus  $\lg(\lambda)$  over 300–550 nm.

227 The solvent effect is not uncommon when measuring aerosol extract absorbance in  
228 difference solvents (Chen and Bond, 2010; Mo et al., 2017; Moschos et al., 2021), but  
229 is rarely accounted for in previous studies. To evaluate the influence of solvent effects  
230 on light absorption of different solvent extracts of the same sample, solutions of 4-  
231 nitrophenol at  $1.90 \text{ mg L}^{-1}$ , 4-nitrocatechol at  $1.84 \text{ mg L}^{-1}$ , and 25-PAH mixtures (Table  
232 S2) at  $0.0080 \text{ mg L}^{-1}$  and  $0.024 \text{ mg L}^{-1}$  (each species) in the five solvents and solvent  
233 mixtures were made up for five times and analyzed for UV/Vis spectra. The absorbance  
234 of PAH mixtures in water was not provided due to their low solubility.

### 235 *2.3 Measurements and analysis of ambient BrC absorption*

236 Collocated  $Q_f$  and  $Q_b$  samples were extracted using the solvent with the highest  $\eta$   
237 value once followed by light absorbance measurement. OC concentrations in  $Q_f$  and  $Q_b$   
238 samples were obtained from Yang et al. (2021), and SEOC values were estimated from  
239 OC concentrations and the average  $\eta$  value determined in *section 2.1* for one-time  
240 extraction. In this work,  $Q_b$  measurements were used to correct  $\text{Abs}_\lambda$ ,  $\text{MAE}_\lambda$ , and  $\text{\AA}$  of  
241 BrC in ambient  $\text{PM}_{2.5}$  in the same manner as those for water and methanol extracts in  
242 Xie et al. (2022)

$$243 \text{ Artifact-corrected } \text{Abs}_\lambda = \text{Abs}_\lambda^{Q_f} - \text{Abs}_\lambda^{Q_b} \quad (4)$$

$$244 \text{ Artifact-corrected } \text{MAE}_\lambda = \frac{\text{Abs}_\lambda^{Q_f} - \text{Abs}_\lambda^{Q_b}}{\text{SEOC}_{Q_f} - \text{OC}_{Q_b}} \quad (5)$$

245 where  $\text{Abs}_\lambda^{Q_f}$  and  $\text{Abs}_\lambda^{Q_b}$  are  $\text{Abs}_\lambda$  values of  $Q_f$  and  $Q_b$  samples, respectively;  $\text{SEOC}_{Q_f}$   
246 represents SEOC concentrations in  $Q_f$  samples;  $\text{OC}_{Q_b}$  denotes OC concentrations in  $Q_b$   
247 samples, assuming that OC in  $Q_b$  is completely dissolved (Xie et al., 2022). Artifact  
248 corrected  $\text{\AA}$  were generated from the regression slope of  $\lg(\text{Abs}_\lambda^{Q_f} - \text{Abs}_\lambda^{Q_b})$  versus  $\lg$   
249  $(\lambda)$  over 300 – 550 nm. Artifact-corrected  $\text{Abs}_\lambda$ ,  $\text{MAE}_\lambda$ , and  $\text{\AA}$  during each sampling

250 interval were determined by averaging each pair of collocated measurements. If one of  
251 the two numbers in a pair is missed, the other number will be directly used for the  
252 specific sampling interval. To compare with previous studies based on water and/or  
253 methanol extraction methods,  $Abs_{\lambda}$  and  $MAE_{\lambda}$  at 365 nm were shown and discussed in  
254 this work.

255 Pearson's correlation coefficient ( $r$ ) was used to show how collocated  
256 measurements of BrC in ambient  $PM_{2.5}$  vary together. The coefficient of divergence  
257 (COD) was calculated to indicate consistency between collocated measurements. The  
258 relative uncertainty of BrC absorption derived from duplicate data was depicted using  
259 the average relative percent difference (ARPD, %), which was used as the uncertainty  
260 fraction for BrC measurements. Calculation methods of COD and ARPD are provided  
261 in Text S1 of supplementary information. To examine the influence of potential BrC  
262 underestimation based on the methanol extraction method on source apportionment,  
263 positive matrix factorization (PMF) version 5.0 (U.S. Environmental Protection  
264 Agency) was applied to attribute the light absorption of aerosol extracts in methanol  
265 and solvent with the highest  $\eta$  to sources. The total concentration data ( $Q_f + Q_b +$   
266 adsorbent) of organic compounds have been used to apportion the light absorption of  
267 MeOH-soluble OC to specific sources (Xie et al., 2022), so as to avoid the impacts of  
268 gas-particle partitioning. In this work, the input particulate bulk components and total  
269 organic molecular marker (OMM) data for PMF analysis were obtained from Xie et al.  
270 (2022) and are summarized in Table S3. Four- to ten-factor solutions were tested to  
271 retrieve a final factor number with the most physically interpretable base-case solution.  
272 More information on input data preparation and the factor number determination are  
273 provided in supplementary information (Text S2 and Table S4).

### 274 **3. Results and discussion**

275 3.1 Solvent test

276 3.1.1 Extraction efficiency of different solvents

277 The concentrations of OC and EC fractions in each sample prior to solvent  
278 extractions are listed in Table S1. SEOC concentrations and extraction efficiencies of  
279 individual solvents and solvent mixtures are detailed in Table 1. Generally, DMF  
280 presented the highest extraction efficiency of total OC whenever filter samples were  
281 extracted once ( $89.0 \pm 7.96\%$ ) or twice ( $95.6 \pm 3.67\%$ ), followed by MeOH (one-time  
282 extraction  $82.3 \pm 8.68\%$ , two-time extraction  $86.6 \pm 7.86\%$ ) and MeOH/DCM mixtures  
283 ( $\sim 75\%$ ,  $\sim 85\%$ ). Although THF and DMF are frequently used to dissolve polymers (e.g.,  
284 polystyrene) for characterization, THF had the lowest  $\eta$  values ( $64.2 \pm 8.08\%$ ,  $70.1 \pm$   
285  $8.01\%$ ) comparable to water ( $66.7 \pm 8.58\%$ ,  $69.9 \pm 5.88\%$ ). Compared with one-time  
286 extraction, the extraction efficiencies of selected solvents were improved by a few  
287 percent when filter samples were extracted twice, and  $\eta$  values of MeOH/DCM  
288 mixtures became closer to those of MeOH (Table 1). These results showed that solvents  
289 can reach more than 80% of their dissolving capacity with the one-time extraction, and  
290 the ambient OC in Nanjing is more soluble in MeOH than in DCM.

291 From OC1 to OC4, the volatility of OC fractions is expected to decrease  
292 continuously, and the molecules in OC fractions evolving at higher temperatures should  
293 be larger than those in OC1 with similar functional groups. In Table 1, MeOH and  
294 MeOH/DCM mixtures had comparable or even higher  $\eta$  values ( $82.6 \pm 25.9\%$ – $97.9 \pm$   
295  $5.02\%$ ) of OC1 and OC2 than DMF ( $88.8 \pm 4.98\%$ – $97.2 \pm 2.12\%$ ). But OC3 and OC4  
296 accounted for more than 60% of OC concentrations, and DMF exhibited significant ( $p$   
297  $< 0.05$ ) larger  $\eta$  values than other solvents, indicating that DMF had stronger dissolving  
298 capacity for large organic molecules than MeOH.

299 Concentrations of extracted OC fractions in MeOH, MeOH/DCM mixtures, and

300 THF based on the two methods for rOC measurements (*section 2.2*) are compared in  
301 Figures S1 and S2. The total SEOC concentrations derived from the two methods are  
302 compared in Figure S3. All the scatter data of SEOC fell along the 1:1 line with  
303 significant correlations ( $r > 0.85$ ,  $p < 0.01$ ). Because the measurement uncertainty of  
304 dominant species is lower than minor ones (Hyslop and White, 2008; Yang et al., 2021),  
305 the slightly greater relative difference between the two methods for extractable OC1  
306 was likely attributed to its low concentrations ( $< 1 \mu\text{g m}^{-3}$ ; Tables 1 and S1). Thus,  
307 baking extracted filters to dryness was expected to have little influence on SEOC  
308 measurements, particularly for low-volatility OC fractions (OC2-OC4).

309 Although water dissolves less OC than MeOH, WSOC is intensively extracted and  
310 analyzed for its composition and light absorption (Hecobian et al., 2010; Liu et al., 2013;  
311 Washenfelder et al., 2015). WSOC can play a significant role in changing the radiative  
312 and cloud-nucleating properties of atmospheric aerosols (Hallar et al., 2013; Taylor et  
313 al., 2017). It also served as a proxy measurement for oxygenated (OOA) or secondary  
314 organic aerosols (SOA) in some regions (Kondo et al., 2007; Weber et al., 2007). In  
315 previous work, MeOH was commonly used as the most efficient solvent in extracting  
316 OC from biomass burning ( $\eta > 90\%$ ; Chen and Bond, 2010; Xie et al., 2017b) and  
317 ambient particles ( $\eta \sim 80\%$ ; Xie et al., 2019b; Xie et al., 2022). MeOH-insoluble OC  
318 has rarely been investigated through direct solvent-extraction followed by instrumental  
319 analysis. There is evidence showing that BrC absorption is associated mostly with large  
320 molecular weight and extremely low-volatility species (Saleh et al., 2014; Di Lorenzo  
321 and Young, 2016; Di Lorenzo et al., 2017). Compared with DMF, the lower capability  
322 of MeOH in dissolving OC3 and OC4 would lead to an underestimation of BrC  
323 absorption in atmospheric aerosols.

324 3.1.2 Light absorption of different solvent extracts

325 Table 2 shows the average  $Abs_{\lambda}$  and  $MAE_{\lambda}$  values of different solvent extracts at  
326 365 and 550 nm. The  $Abs_{\lambda}$  and  $MAE_{\lambda}$  spectra of selected samples are illustrated in  
327 Figure S4. Not including DMF, MeOH extracts exhibited the strongest light absorption.  
328 Since MeOH can dissolve more OC3 and OC4 than DCM (Table 1), the  $Abs_{\lambda}$  and  $MAE_{\lambda}$   
329 of MeOH/DCM extracts decreased as the fraction of DCM increased in solvent  
330 mixtures (Table 2 and Figure S4). Water and THF extracts had the smallest  $Abs_{\lambda}$  and  
331  $MAE_{\lambda}$  due to their low extraction efficiencies for low-volatility OC (OC2-OC4; Table  
332 1). In comparison to MeOH extracts,  $Abs_{365/550}$  and  $MAE_{365/550}$  of DMF extracts were  
333 at least more than 40% higher ( $p < 0.05$ ). Given that the relative difference in extraction  
334 efficiency of total OC between MeOH and DMF was less than 10% and DMF dissolved  
335 more OC3 and OC4 than other solvents (Table 1), low-volatility OC should contain  
336 stronger light-absorbing chromophores (Saleh et al., 2014) and its mass fraction might  
337 determine the difference in BrC absorption across solvent extraction methods.  
338 Moreover, the relative difference in  $Abs_{\lambda}$  and  $MAE_{\lambda}$  between MeOH and DMF extracts  
339 increased with wavelength (Table 2 and Figure S4). This is because the light absorption  
340 of DMF extracts that contain stronger BrC chromophores depends less on wavelengths  
341 than other solvent extracts ( $\bar{A} \sim 4.5$ , Table 2). As shown in Figure S5, average  $\bar{A}$  and  
342  $MAE_{365/550}$  values of individual solvent extracts in Table 2 are negatively correlated.

343 In this work, insoluble organic particles coming off the filter during sonication  
344 might lead to overestimated SEOC concentrations and  $\eta$  values, and then the  $MAE_{\lambda}$  of  
345 solvent extracts would be underestimated. Previous studies rarely considered the loss  
346 of insoluble OC during the extraction process (Yan et al., 2020), of which the impact  
347 on  $MAE_{\lambda}$  calculation was still inconclusive. But  $Abs_{\lambda}$  measurements would never be  
348 influenced, as the light absorbance of solvent extracts was analyzed after filtration. In  
349 Table 2, the second extraction only increases the average  $Abs_{365}$  and  $Abs_{550}$  values of

350 DMF extracts by 6.70% ( $p = 0.78$ ) and 6.76% ( $p = 0.77$ ), respectively. We suspected  
351 that the difference in  $\eta$  values of DMF between one-time and two-time extraction  
352 procedures was mainly ascribed to the detachment of insoluble OC particles.

353 In Figure S6, the absorbance spectra of 4-nitrophenol and 4-nitrocatechol in water  
354 shift toward longer wavelengths compared to their MeOH solution. This is because  
355 neutral and deprotonated forms of 4-nitrophenol and 4-nitrocatechol may have different  
356 absorbance spectra, and these two compounds are deprotonated at  $\text{pH} \approx 7$  (Lin et al.,  
357 2015b, 2017). The strong light absorption of 4-nitrophenol and 4-nitrocatechol in DMF  
358 at 450 nm was not observed in other solvents, and was likely caused by unknown  
359 reactions. Then the solvent effect introduced by DMF might overestimate the light  
360 absorption of low-molecular-weight (LMW) nitrophenol-like species at  $> 400$  nm in  
361 source or ambient aerosols. Evidence shows that BrC absorption is dominated by large  
362 molecules with extremely low volatility (Saleh et al., 2014; Di Lorenzo and Young,  
363 2016; Di Lorenzo et al., 2017), and LMW nitrophenol-like species have very low  
364 contributions to particulate OM (e.g.,  $< 1\%$ ) and aerosol extract absorption (e.g.,  $< 10\%$ )  
365 (Mohr et al., 2013; Zhang et al., 2013; Teich et al., 2017; Xie et al., 2019a, 2020; Li et  
366 al., 2020). The shapes of the light absorption spectra of aerosol extracts in DMF were  
367 similar to other solvents (Figure S4) and PAH solutions (Figure S6g-1), and no elevation  
368 in light absorption appeared at 400–500 nm. Thus, the overestimated absorption of  
369 LMW nitrophenol-like species in DMF might not substantially impact the overall BrC  
370 absorption of aerosol extracts. Furthermore, the absorbance of 4-nitrophenol and 4-  
371 nitrocatechol in DMF at 365 nm ( $A_{365}$ ) was lower than that in MeOH, and PAH  
372 solutions showed very similar absorbance spectra across the five solvents (Figure S6g-  
373 1 and Table S5). Considering that low-volatility OC fractions (e.g., OC3 and OC4) in  
374 the ambient are less water soluble (Table 1) and have a high degree of conjugation

375 (Chen and Bond, 2010; Lin et al., 2014), their structures are probably featured by a  
376 PAH skeleton. Therefore, the large difference in  $Abs_{365}$  between DMF and MeOH  
377 extracts (Table 2) was primarily ascribed to the fact that DMF can dissolve more OC3  
378 and OC4 than methanol (Table 1). However, we cannot rule out the impact of solvent  
379 effects on the comparison of light absorption spectra between MeOH and DMF extracts  
380 (Figure S4), and more work is warranted in identifying the structures more soluble in  
381 DMF than in MeOH.

### 382 *3.2 Collocated measurements and temporal variability*

383  $Abs_{365}$  values of collocated  $Q_f$  and  $Q_b$  extracts in DMF are summarized in Table S6.  
384 No significant difference was observed ( $Q_f$   $p = 0.96$ ;  $Q_b$   $p = 0.42$ ) between the two  
385 samplers. After  $Q_b$  corrections,  $Abs_{365}$ ,  $MAE_{365}$ , and  $\dot{A}$  of DMF extractable OC ( $Abs_{365,d}$ ,  
386  $MAE_{365,d}$ , and  $\dot{A}_d$ ) in  $PM_{2.5}$  were calculated by averaging each pair of duplicate  $Q_f$ - $Q_b$   
387 data, and are compared with those of methanol extracts ( $Abs_{365,m}$ ,  $MAE_{365,m}$ , and  $\dot{A}_m$ )  
388 in Table 3. Figure 1 shows comparisons between collocated measurements of  $Abs_{365,d}$ ,  
389  $MAE_{365,d}$ , and  $\dot{A}_d$ . Generally, all comparisons indicated good agreement with  $COD <$   
390  $0.20$  ( $0.094$ – $0.15$ ).  $Abs_{365,d}$  and  $MAE_{365,d}$  had comparable uncertainty fractions (ARPD,  
391  $22.7\%$  and  $24.5\%$ , Figure 1) as  $Abs_{365,m}$  and  $MAE_{365,m}$  ( $28.4\%$  and  $28.8\%$ ; Xie et al.,  
392 2022). Since different primary combustion sources can have similar spectral  
393 dependence for BrC absorption (Chen and Bond, 2010; Xie et al., 2017b; Xie et al.,  
394 2018; Xie et al., 2019a), most  $\dot{A}_d$  data clustered on the identity line with much lower  
395 variability than  $Abs_{365,d}$  and  $MAE_{365,d}$ . As shown in Table 3, average  $Abs_{365,d}$  and  
396  $MAE_{365,d}$  values were  $30.7\%$  ( $p < 0.01$ ) and  $17.3\%$  ( $p < 0.05$ ) larger than average  
397  $Abs_{365,m}$  and  $MAE_{365,m}$ . Because the  $k$  value of BrC in bulk solution is directly estimated  
398 from  $Abs_\lambda$  or  $MAE_\lambda$  (Liu et al., 2013; Liu et al., 2016; Lu et al., 2015), the estimation  
399 method needs to be revised when ambient BrC is extracted using DMF instead of



400 MeOH. Both  $MAE_{365,d}$  and  $MAE_{365,m}$  were negatively correlated ( $p < 0.01$ ) with their  
401 corresponding  $\hat{A}$  values (Figure S7), and the lower average  $\hat{A}_d$  ( $5.25 \pm 0.64$ ,  $p < 0.01$ )  
402 compared to  $\hat{A}_m$  ( $6.81 \pm 1.64$ ; Table 3) supports that more-absorbing BrC had less  
403 spectral dependence than less-absorbing BrC.

404 Figure 2 compares the time series of  $Abs_{365}$ ,  $MAE_{365}$ , and  $\hat{A}$  between the DMF and  
405 MeOH extracts. Both DMF and MeOH extracts had significant ( $p < 0.05$ ) higher  
406 absorption at night-time than during the daytime due to the “photo-bleaching” effect  
407 (Zhang et al., 2020; Xie et al., 2022). All the three parameters of DMF and MeOH  
408 extracts exhibited consistency in winter (Figure 2) when biomass burning dominated  
409 BrC absorption (Xie et al., 2022). While in later spring and summer (2019/05/15–  
410 2019/08/01), average  $Abs_{365,d}$  and  $MAE_{365,d}$  values were more than two times greater  
411 than the average  $Abs_{365,m}$  and  $MAE_{365,m}$ . Many studies have identified a temporal  
412 pattern of BrC absorption with winter maxima and summer minima based on  
413 water/MeOH extraction methods (Lukács et al., 2007; Zhang et al., 2010; Du et al.,  
414 2014; Zhu et al., 2018). Due to the low capability of water and MeOH in dissolving  
415 large BrC molecules, BrC absorption and its temporal variations in these studies might  
416 be biased. Moreover, the identification of BrC sources using receptor models is highly  
417 dependent on the difference in the time series of input species (Dall'Osto et al., 2013).  
418 Then, using DMF instead of MeOH for BrC extraction and measurements will lead to  
419 distinct source apportionment results.

### 420 *3.3 Sources of DMF and MeOH Extractable BrC*

421 A final factor number of eight was determined based on the interpretability of  
422 different base-case solutions (four to ten factors), the change in  $Q/Q_{exp}$  with factor  
423 numbers, and robustness analysis (Text S2 and Table S4). Normalized factor profiles of  
424 seven- to nine-factor solutions are compared in Figure S8. The seven-factor solution

425 failed to resolve the lubricating oil combustion factor characterized by hopanes and  
426 steranes (Figure S8c). An unknown factor containing various source tracers related to  
427 crustal dust ( $\text{Ca}^{2+}$  and  $\text{Mg}^{2+}$ ), lubricating oil (hopanes and steranes), and soil microbiota  
428 (sugar and sugar alcohols) was identified in the nine-factor solution (Figure S8i).  
429 Median and mean values of input  $\text{Abs}_{365,\text{d}}$ ,  $\text{Abs}_{365,\text{m}}$ , and bulk component concentrations  
430 agreed well with PMF estimations (Table S7), and the strong correlations ( $r = 0.86$ –  
431  $0.99$ ) between observations and PMF estimations indicated that the eight-factor  
432 solution simulated the time series of input species well. In comparison to Xie et al.  
433 (2022), where  $\text{Abs}_{365}$  of MeOH and water extracts were apportioned to nine sources  
434 using the same speciation data, this work lumped secondary nitrate and sulfate to the  
435 same factor (termed “secondary inorganics”, Figure S8h), and the other seven factors  
436 had similar factor profiles linked with biomass burning, non-combustion fossil,  
437 lubricating oil combustion, coal combustion, dust resuspension, biogenic emission, and  
438 isoprene oxidation. Interpretations of individual factors based on characteristic source  
439 tracers and contribution time series were provided in previous work (Gou et al., 2021;  
440 Xie et al., 2022).

441 The average relative contributions of the identified factors to  $\text{Abs}_{365,\text{d}}$ ,  $\text{Abs}_{365,\text{m}}$ , and  
442 bulk components are listed in Table S8. Consistent contribution distributions of  $\text{Abs}_{365,\text{m}}$   
443 were observed between Xie et al. (2022) and this study, indicating that the PMF results  
444 were robust to the inclusion of  $\text{Abs}_{365,\text{d}}$  data. Figure 3 compares the time series of factor  
445 contributions to  $\text{Abs}_{365,\text{d}}$  and  $\text{Abs}_{365,\text{m}}$ . ARPD and COD values between factor  
446 contributions to  $\text{Abs}_{365,\text{d}}$  and  $\text{Abs}_{365,\text{m}}$  and the absolute difference are exhibited in Figure  
447 S9.  $\text{Abs}_{365,\text{d}}$  and  $\text{Abs}_{365,\text{m}}$  had comparable contributions from biomass burning,  
448 lubricating oil combustion, and coal combustion (Figure 3a, c, d). The small COD  
449 values of these three factors (0.0041–0.17) indicated no significant divergence. The

450 biogenic emission and isoprene oxidation factors exhibited complete difference (ARPD  
451 = 200%, COD = 1; Figure S9f, g) as they had no contribution to Abs<sub>365,m</sub>. Among the  
452 eight factors, the non-combustion fossil, dust resuspension, and isoprene oxidation  
453 factors had the largest median difference in factor contributions to Abs<sub>365,d</sub> and Abs<sub>365,m</sub>  
454 (0.63–0.67 Mm<sup>-1</sup>) with substantial heterogeneity (COD > 0.20), followed by the  
455 secondary inorganics factor (0.20 Mm<sup>-1</sup>, COD = 0.41). The temporal variations of the  
456 absolute difference shown in Figure S9 are identical to the contributions of individual  
457 factors to Abs<sub>365,d</sub> or Abs<sub>365,m</sub> (Figure 3).

458 The non-combustion fossil factor represents unburned fossil-fuel emissions (e.g.,  
459 petroleum products), which contain substantial large organic molecules (e.g., high MW  
460 PAHs; Simoneit and Fetzer, 1996; Mi et al., 2000). This might explain why the non-  
461 combustion fossil factor contributed more Abs<sub>365,d</sub> than Abs<sub>365,m</sub> all over the year  
462 (Figure S9b). Dust resuspension and isoprene oxidation factors show prominent  
463 contributions to Abs<sub>365,d</sub> in spring and summer, respectively (Figure 3e, g). The dust  
464 resuspension factor had the highest average contributions to both crustal materials (Ca<sup>2+</sup>  
465 and Mg<sup>2+</sup>) and carbonaceous species (OC and EC; Table S8 and Figure S8), and was  
466 considered a mixed source of crustal dust and motor vehicle emissions (Yu et al., 2020;  
467 Xie et al., 2022). Besides the influences from primary emissions, aging processes of  
468 organic components in dust aerosols can induce the formation of BrC through iron-  
469 catalyzed polymerization (Link et al., 2020; Al-Abadleh, 2021; Chin et al., 2021). It  
470 was demonstrated that the isoprene-derived polymerization products through aerosol-  
471 phase reactions are light-absorbing chromophores (Lin et al., 2014; Nakayama et al.,  
472 2015). This might explain the elevated difference between Abs<sub>365,d</sub> and Abs<sub>365,m</sub>  
473 contributions of the isoprene oxidation factor in summer (Figure S9g). The biogenic  
474 emission factor was characterized by tracers related to microbiota activities (sugar and

475 sugar alcohols) and decomposition of high plant materials (odd-numbered alkanes) in  
476 soil (Rogge et al., 1993; Simoneit et al., 2004), and had negligible contributions (< 0.1%)  
477 to Abs<sub>365,d</sub> and Abs<sub>365,m</sub>. Evidence shows that secondary BrC can be generated through  
478 gas-phase reactions of anthropogenic volatile organic compounds with NO<sub>x</sub>  
479 (Nakayama et al., 2010; Liu et al., 2016; Xie et al., 2017a), aqueous reactions of SOA  
480 with reduced nitrogen-containing species (e.g., NH<sub>4</sub><sup>+</sup>; Updyke et al., 2012; Powelson et  
481 al., 2014; Lin et al., 2015a), and evaporation of water from droplets in the atmosphere  
482 containing soluble organics (Nguyen et al., 2012; Kasthuriarachchi et al., 2020). These  
483 processes can also lead to the formation of low-volatility oligomers (Nguyen et al.,  
484 2012; Song et al., 2013), and their contributions might be lumped into the secondary  
485 inorganics factor due to the lack of OMMs. According to these results, one possible  
486 explanation for the difference in time series between Abs<sub>365,d</sub> and Abs<sub>365,m</sub> (Figure 2) is  
487 that large BrC molecules from unburned fossil fuels and atmospheric processes are less  
488 soluble in MeOH than in DMF.

#### 489 **4. Conclusions and implications**

490 Comparisons of extraction efficiencies and light absorption of ambient aerosol  
491 extracts across selected solvents and solvent mixtures indicate that MeOH may  
492 sometimes be replaced with DMF for measuring BrC absorption, as low-volatility OC  
493 fractions containing strong chromophores are less soluble in MeOH than in DMF.  
494 Existing modeling studies on the radiative forcing of BrC (Feng et al., 2013; Wang et  
495 al., 2014; Zhang et al., 2020) often retrieved or estimated its optical properties from  
496 laboratory or ambient measurements based on water/methanol extraction methods  
497 (Chen and Bond, 2010; Hecobian et al., 2010; Liu et al., 2013; Zhang et al., 2013), and  
498 had a potential to underestimate the contribution of BrC to total aerosol absorption.  
499 However, the influence of the solvent effect was not accounted for in this work when

500 comparing the light absorption of different solvent extracts. The difference between  
501 MeOH and DMF extract absorption might change with the time and location due to the  
502 variations in BrC sources. The results of this work also imply the necessity of applying  
503 different solvents or combinations of solvents with broad polarity and dissolving  
504 capability to study BrC composition and absorption, particularly for low-volatility  
505 fractions.

506 Although light-absorbing properties of DMF and MeOH extracts had good  
507 agreement in cold periods, when biomass and coal burning sources dominated BrC  
508 emissions, their distinct time series in spring and summer implies that the contributions  
509 of certain BrC sources were underestimated or missed when the MeOH extraction  
510 method was used. Source apportionment results of Abs<sub>365,d</sub> and Abs<sub>365,m</sub> based on  
511 organic molecular marker data indicated that large and methanol insoluble BrC  
512 molecules are likely coming from unburned fossil fuels and polymerization of aerosol  
513 organics. Laboratory studies have observed the polymerization process through  
514 heterogeneous reactions of several precursors (e.g., catechol; Lin et al., 2014; Link et  
515 al., 2020), but the structures and light-absorbing properties of potential polymerization  
516 products in ambient aerosols (Figure 3e, g) are less understood and warrant further  
517 study.

518

#### 519 ***Data availability***

520 Data used in the writing of this paper is available at the Harvard Dataverse  
521 (<https://doi.org/10.7910/DVN/CGHPXB>, Xu et al., 2022)

522

#### 523 ***Author contributions***

524 MX designed the research. ZX, WF, YW, and HY performed laboratory experiments.

525 ZX, WF, and MX analyzed the data. ZX and MX wrote the paper with significant  
526 contributions from YW and HL.

527

### 528 *Competing interests*

529 The authors declare that they have no conflict of interest.

530

### 531 *Acknowledgments*

532 This work was supported by the National Natural Science Foundation of China  
533 (NSFC, 42177211, 41701551).

534

### 535 **References**

- 536 Al-Abadleh, H. A.: Aging of atmospheric aerosols and the role of iron in catalyzing brown carbon  
537 formation, *Environ. Sci.: Atmos.*, 1, 297-345, 10.1039/D1EA00038A, 2021.
- 538 Atwi, K., Cheng, Z., El Hajj, O., Perrie, C., and Saleh, R.: A dominant contribution to light absorption  
539 by methanol-insoluble brown carbon produced in the combustion of biomass fuels typically  
540 consumed in wildland fires in the United States, *Environ. Sci.: Atmos.*, 10.1039/D1EA00065A, 2022.
- 541 Bai, Z., Zhang, L., Cheng, Y., Zhang, W., Mao, J., Chen, H., Li, L., Wang, L., and Chen, J.:  
542 Water/methanol-insoluble brown carbon can dominate aerosol-enhanced light absorption in port  
543 cities, *Environ. Sci. Technol.*, 54, 14889-14898, 10.1021/acs.est.0c03844, 2020.
- 544 Chen, Y., and Bond, T. C.: Light absorption by organic carbon from wood combustion, *Atmos. Chem.*  
545 *Phys.*, 10, 1773-1787, 10.5194/acp-10-1773-2010, 2010.
- 546 Cheng, Z., Atwi, K., Hajj, O. E., Ijeli, I., Fischer, D. A., Smith, G., and Saleh, R.: Discrepancies between  
547 brown carbon light-absorption properties retrieved from online and offline measurements, *Aerosol*  
548 *Sci. Technol.*, 55, 92-103, 10.1080/02786826.2020.1820940, 2021.
- 549 Chin, H., Hopstock, K. S., Fleming, L. T., Nizkorodov, S. A., and Al-Abadleh, H. A.: Effect of aromatic  
550 ring substituents on the ability of catechol to produce brown carbon in iron(iii)-catalyzed reactions,  
551 *Environ. Sci.: Atmos.*, 1, 64-78, 10.1039/D0EA00007H, 2021.
- 552 Dall'Osto, M., Querol, X., Amato, F., Karanasiou, A., Lucarelli, F., Nava, S., Calzolari, G., and Chiari,  
553 M.: Hourly elemental concentrations in PM<sub>2.5</sub> aerosols sampled simultaneously at urban  
554 background and road site during SAPUSS – diurnal variations and PMF receptor modelling, *Atmos.*  
555 *Chem. Phys.*, 13, 4375-4392, 10.5194/acp-13-4375-2013, 2013.
- 556 Di Lorenzo, R. A., and Young, C. J.: Size separation method for absorption characterization in brown  
557 carbon: Application to an aged biomass burning sample, *Geophys. Res. Lett.*, 43, 458-465,  
558 10.1002/2015gl066954, 2016.
- 559 Di Lorenzo, R. A., Washenfelder, R. A., Attwood, A. R., Guo, H., Xu, L., Ng, N. L., Weber, R. J.,  
560 Baumann, K., Edgerton, E., and Young, C. J.: Molecular-size-separated brown carbon absorption for  
561 biomass-burning aerosol at multiple field sites, *Environ. Sci. Technol.*, 51, 3128-3137,  
562 10.1021/acs.est.6b06160, 2017.
- 563 Du, Z., He, K., Cheng, Y., Duan, F., Ma, Y., Liu, J., Zhang, X., Zheng, M., and Weber, R.: A yearlong  
564 study of water-soluble organic carbon in Beijing I: Sources and its primary vs. secondary nature,  
565 *Atmos. Environ.*, 92, 514-521, <https://doi.org/10.1016/j.atmosenv.2014.04.060>, 2014.
- 566 Feng, Y., Ramanathan, V., and Kotamarthi, V. R.: Brown carbon: a significant atmospheric absorber of  
567 solar radiation? *Atmos. Chem. Phys.*, 13, 8607-8621, 10.5194/acp-13-8607-2013, 2013.
- 568 Gou, Y., Qin, C., Liao, H., and Xie, M.: Measurements, gas/particle partitioning, and sources of nonpolar

569 organic molecular markers at a suburban site in the west Yangtze River Delta, China, *J. Geophys.*  
570 *Res. Atmos.*, 126, e2020JD034080, <https://doi.org/10.1029/2020JD034080>, 2021.

571 Hallar, A. G., Lowenthal, D. H., Clegg, S. L., Samburova, V., Taylor, N., Mazzoleni, L. R., Zielinska, B.  
572 K., Kristensen, T. B., Chirokova, G., McCubbin, I. B., Dodson, C., and Collins, D.: Chemical and  
573 hygroscopic properties of aerosol organics at Storm Peak Laboratory, *J. Geophys. Res. Atmos.*, 118,  
574 4767-4779, <https://doi.org/10.1002/jgrd.50373>, 2013.

575 Hecobian, A., Zhang, X., Zheng, M., Frank, N., Edgerton, E. S., and Weber, R. J.: Water-Soluble Organic  
576 Aerosol material and the light-absorption characteristics of aqueous extracts measured over the  
577 Southeastern United States, *Atmos. Chem. Phys.*, 10, 5965-5977, 10.5194/acp-10-5965-2010, 2010.

578 Hems, R. F., Schnitzler, E. G., Liu-Kang, C., Cappa, C. D., and Abbatt, J. P. D.: Aging of atmospheric  
579 brown carbon aerosol, *ACS Earth Space Chem.*, 5, 722-748, 10.1021/acsearthspacechem.0c00346,  
580 2021.

581 Huang, R.-J., Yang, L., Cao, J., Chen, Y., Chen, Q., Li, Y., Duan, J., Zhu, C., Dai, W., Wang, K., Lin, C.,  
582 Ni, H., Corbin, J. C., Wu, Y., Zhang, R., Tie, X., Hoffmann, T., O'Dowd, C., and Dusek, U.: Brown  
583 carbon aerosol in urban Xi'an, northwest China: The composition and light absorption properties,  
584 *Environ. Sci. Technol.*, 52, 6825-6833, 10.1021/acs.est.8b02386, 2018.

585 Huang, R.-J., Yang, L., Shen, J., Yuan, W., Gong, Y., Guo, J., Cao, W., Duan, J., Ni, H., Zhu, C., Dai, W.,  
586 Li, Y., Chen, Y., Chen, Q., Wu, Y., Zhang, R., Dusek, U., O'Dowd, C., and Hoffmann, T.: Water-  
587 insoluble organics dominate brown carbon in wintertime urban aerosol of China: Chemical  
588 characteristics and optical properties, *Environ. Sci. Technol.*, 54, 7836-7847,  
589 10.1021/acs.est.0c01149, 2020.

590 Hyslop, N. P., and White, W. H.: An evaluation of interagency monitoring of protected visual  
591 environments (IMPROVE) collocated precision and uncertainty estimates, *Atmos. Environ.*, 42,  
592 2691-2705, <https://doi.org/10.1016/j.atmosenv.2007.06.053>, 2008.

593 Kasthuriarachchi, N. Y., Rivellini, L.-H., Chen, X., Li, Y. J., and Lee, A. K. Y.: Effect of relative humidity  
594 on secondary brown carbon formation in aqueous droplets, *Environ. Sci. Technol.*, 54, 13207-13216,  
595 10.1021/acs.est.0c01239, 2020.

596 Kondo, Y., Miyazaki, Y., Takegawa, N., Miyakawa, T., Weber, R. J., Jimenez, J. L., Zhang, Q., and  
597 Worsnop, D. R.: Oxygenated and water-soluble organic aerosols in Tokyo, *J. Geophys. Res. Atmos.*,  
598 112, D01203, 10.1029/2006jd007056, 2007.

599 Lack, D. A., Langridge, J. M., Bahreini, R., Cappa, C. D., Middlebrook, A. M., and Schwarz, J. P.: Brown  
600 carbon and internal mixing in biomass burning particles, *Proc. Natl. Acad. Sci. U.S.A.*, 109, 14802-  
601 14807, 10.1073/pnas.1206575109, 2012.

602 Laskin, A., Laskin, J., and Nizkorodov, S. A.: Chemistry of atmospheric brown carbon, *Chem. Rev.*, 115,  
603 4335-4382, 10.1021/cr5006167, 2015.

604 Li, X., Yang, Y., Liu, S., Zhao, Q., Wang, G., and Wang, Y.: Light absorption properties of brown carbon  
605 (BrC) in autumn and winter in Beijing: Composition, formation and contribution of nitrated aromatic  
606 compounds, *Atmos. Environ.*, 223, 117289, <https://doi.org/10.1016/j.atmosenv.2020.117289>, 2020.

607 Li, Y., Ji, Y., Zhao, J., Wang, Y., Shi, Q., Peng, J., Wang, Y., Wang, C., Zhang, F., Wang, Y., Seinfeld, J.  
608 H., and Zhang, R.: Unexpected oligomerization of small  $\alpha$ -dicarbonyls for secondary organic aerosol  
609 and brown carbon formation, *Environ. Sci. Technol.*, 55, 4430-4439, 10.1021/acs.est.0c08066, 2021.

610 Lin, P., Laskin, J., Nizkorodov, S. A., and Laskin, A.: Revealing brown carbon chromophores produced  
611 in reactions of methylglyoxal with ammonium sulfate, *Environ. Sci. Technol.*, 49, 14257-14266,  
612 10.1021/acs.est.5b03608, 2015a

613 Lin, P., Liu, J. M., Shilling, J. E., Kathmann, S. M., Laskin, J., and Laskin, A.: Molecular characterization  
614 of brown carbon (BrC) chromophores in secondary organic aerosol generated from photo-oxidation  
615 of toluene, *Phys. Chem. Chem. Phys.*, 17, 23312-23325, 10.1039/c5cp02563j, 2015b.

616 Lin, P., Bluvshstein, N., Rudich, Y., Nizkorodov, S. A., Laskin, J., and Laskin, A.: Molecular chemistry of  
617 atmospheric brown carbon inferred from a nationwide biomass burning event, *Environ. Sci. Technol.*,  
618 51, 11561-11570, 10.1021/acs.est.7b02276, 2017.

619 Lin, P., Aiona, P. K., Li, Y., Shiraiwa, M., Laskin, J., Nizkorodov, S. A., and Laskin, A.: Molecular  
620 characterization of brown carbon in biomass burning aerosol particles, *Environ. Sci. Technol.*, 50,  
621 11815-11824, 10.1021/acs.est.6b03024, 2016.

622 Lin, Y.-H., Budisulistiorini, S. H., Chu, K., Siejack, R. A., Zhang, H., Riva, M., Zhang, Z., Gold, A.,  
623 Kautzman, K. E., and Surratt, J. D.: Light-absorbing oligomer formation in secondary organic  
624 aerosol from reactive uptake of isoprene epoxydiols, *Environ. Sci. Technol.*, 48, 12012-12021,  
625 10.1021/es503142b, 2014.

626 Link, N., Removski, N., Yun, J., Fleming, L. T., Nizkorodov, S. A., Bertram, A. K., and Al-Abadleh, H.  
627 A.: Dust-catalyzed oxidative polymerization of catechol and its impacts on ice nucleation efficiency

628 and optical properties, *ACS Earth Space Chem.*, 4, 1127-1139, 10.1021/acsearthspacechem.0c00107,  
629 2020.

630 Liu, J., Bergin, M., Guo, H., King, L., Kotra, N., Edgerton, E., and Weber, R. J.: Size-resolved  
631 measurements of brown carbon in water and methanol extracts and estimates of their contribution to  
632 ambient fine-particle light absorption, *Atmos. Chem. Phys.*, 13, 12389-12404, 10.5194/acp-13-  
633 12389-2013, 2013.

634 Liu, J., Lin, P., Laskin, A., Laskin, J., Kathmann, S. M., Wise, M., Caylor, R., Imholt, F., Selimovic, V.,  
635 and Shilling, J. E.: Optical properties and aging of light-absorbing secondary organic aerosol, *Atmos.*  
636 *Chem. Phys.*, 16, 12815-12827, 10.5194/acp-16-12815-2016, 2016.

637 Lu, Z., Streets, D. G., Winijkul, E., Yan, F., Chen, Y., Bond, T. C., Feng, Y., Dubey, M. K., Liu, S., Pinto,  
638 J. P., and Carmichael, G. R.: Light absorption properties and radiative effects of primary organic  
639 aerosol emissions, *Environ. Sci. Technol.*, 49, 4868-4877, 10.1021/acs.est.5b00211, 2015.

640 Lukács, H., Gelencsér, A., Hammer, S., Puxbaum, H., Pio, C., Legrand, M., Kasper-Giebl, A., Handler,  
641 M., Limbeck, A., Simpson, D., and Preunkert, S.: Seasonal trends and possible sources of brown  
642 carbon based on 2-year aerosol measurements at six sites in Europe, *J. Geophys. Res. Atmos.*, 112,  
643 <https://doi.org/10.1029/2006JD008151>, 2007.

644 Mack, L. A., Levin, E. J. T., Kreidenweis, S. M., Obrist, D., Moosmüller, H., Lewis, K. A., Arnott, W. P.,  
645 McMeeking, G. R., Sullivan, A. P., Wold, C. E., Hao, W. M., Collett Jr, J. L., and Malm, W. C.:  
646 Optical closure experiments for biomass smoke aerosols, *Atmos. Chem. Phys.*, 10, 9017-9026,  
647 10.5194/acp-10-9017-2010, 2010.

648 Mo, Y., Li, J., Liu, J., Zhong, G., Cheng, Z., Tian, C., Chen, Y., and Zhang, G.: The influence of solvent  
649 and pH on determination of the light absorption properties of water-soluble brown carbon, *Atmos.*  
650 *Environ.*, 161, 90-98, <https://doi.org/10.1016/j.atmosenv.2017.04.037>, 2017.

651 Mohr, C., Lopez-Hilfiker, F. D., Zotter, P., Prévôt, A. S. H., Xu, L., Ng, N. L., Herndon, S. C., Williams,  
652 L. R., Franklin, J. P., Zahniser, M. S., Worsnop, D. R., Knighton, W. B., Aiken, A. C., Gorkowski,  
653 K. J., Dubey, M. K., Allan, J. D., and Thornton, J. A.: Contribution of nitrated phenols to wood  
654 burning brown carbon light absorption in Detling, United Kingdom during winter time, *Environ. Sci.*  
655 *Technol.*, 47, 6316-6324, 10.1021/es400683v, 2013.

656 Moschos, V., Gysel-Beer, M., Modini, R. L., Corbin, J. C., Massabò, D., Costa, C., Danelli, S. G.,  
657 Vlachou, A., Daellenbach, K. R., Szidat, S., Prati, P., Prévôt, A. S. H., Baltensperger, U., and El  
658 Haddad, I.: Source-specific light absorption by carbonaceous components in the complex aerosol  
659 matrix from yearly filter-based measurements, *Atmos. Chem. Phys.*, 21, 12809-12833, 10.5194/acp-  
660 21-12809-2021, 2021.

661 Mi, H.-H., Lee, W.-J., Chen, C.-B., Yang, H.-H., and Wu, S.-J.: Effect of fuel aromatic content on PAH  
662 emission from a heavy-duty diesel engine, *Chemosphere*, 41, 1783-1790,  
663 [https://doi.org/10.1016/S0045-6535\(00\)00043-6](https://doi.org/10.1016/S0045-6535(00)00043-6), 2000.

664 Nakayama, T., Matsumi, Y., Sato, K., Imamura, T., Yamazaki, A., and Uchiyama, A.: Laboratory studies  
665 on optical properties of secondary organic aerosols generated during the photooxidation of toluene  
666 and the ozonolysis of  $\alpha$ -pinene, *J. Geophys. Res. Atmos.*, 115, D24204, 10.1029/2010jd014387,  
667 2010.

668 Nakayama, T., Sato, K., Tsuge, M., Imamura, T., and Matsumi, Y.: Complex refractive index of secondary  
669 organic aerosol generated from isoprene/NO<sub>x</sub> photooxidation in the presence and absence of SO<sub>2</sub>,  
670 *J. Geophys. Res. Atmos.*, 120, 7777-7787, <https://doi.org/10.1002/2015JD023522>, 2015.

671 Nguyen, T. B., Lee, P. B., Updyke, K. M., Bones, D. L., Laskin, J., Laskin, A., and Nizkorodov, S. A.:  
672 Formation of nitrogen- and sulfur-containing light-absorbing compounds accelerated by evaporation  
673 of water from secondary organic aerosols, *J. Geophys. Res. Atmos.*, 117, D01207,  
674 10.1029/2011jd016944, 2012.

675 Powelson, M. H., Espelien, B. M., Hawkins, L. N., Galloway, M. M., and De Haan, D. O.: Brown carbon  
676 formation by aqueous-phase carbonyl compound reactions with amines and ammonium sulfate,  
677 *Environ. Sci. Technol.*, 48, 985-993, 10.1021/es4038325, 2014.

678 Qin, C., Gou, Y., Wang, Y., Mao, Y., Liao, H., Wang, Q., and Xie, M.: Gas-particle partitioning of polyol  
679 tracers at a suburban site in Nanjing, east China: increased partitioning to the particle phase, *Atmos.*  
680 *Chem. Phys.*, 21, 12141-12153, 10.5194/acp-21-12141-2021, 2021.

681 Rogge, W. F., Hildemann, L. M., Mazurek, M. A., Cass, G. R., and Simoneit, B. R. T.: Sources of fine  
682 organic aerosol .4. Particulate abrasion products from leaf surfaces of urban plants, *Environ. Sci.*  
683 *Technol.*, 27, 2700-2711, 10.1021/es00049a008, 1993.

684 Saleh, R., Hennigan, C. J., McMeeking, G. R., Chuang, W. K., Robinson, E. S., Coe, H., Donahue, N.  
685 M., and Robinson, A. L.: Absorptivity of brown carbon in fresh and photo-chemically aged biomass-  
686 burning emissions, *Atmos. Chem. Phys.*, 13, 7683-7693, 10.5194/acp-13-7683-2013, 2013.



687 Saleh, R., Robinson, E. S., Tkacik, D. S., Ahern, A. T., Liu, S., Aiken, A. C., Sullivan, R. C., Presto, A.  
688 A., Dubey, M. K., Yokelson, R. J., Donahue, N. M., and Robinson, A. L.: Brownness of organics in  
689 aerosols from biomass burning linked to their black carbon content, *Nat. Geosci.*, 7, 647-650,  
690 <https://doi.org/10.1038/ngeo2220>, 2014.

691 Saleh, R.: From measurements to models: Toward accurate representation of brown carbon in climate  
692 calculations, *Curr. Pollut. Rep.*, 6, 90-104, [10.1007/s40726-020-00139-3](https://doi.org/10.1007/s40726-020-00139-3), 2020.

693 Schauer, J. J., Mader, B. T., Deminter, J. T., Heidemann, G., Bae, M. S., Seinfeld, J. H., Flagan, R. C.,  
694 Cary, R. A., Smith, D., Huebert, B. J., Bertram, T., Howell, S., Kline, J. T., Quinn, P., Bates, T.,  
695 Turpin, B., Lim, H. J., Yu, J. Z., Yang, H., and Keywood, M. D.: ACE-Asia intercomparison of a  
696 thermal-optical method for the determination of particle-phase organic and elemental carbon,  
697 *Environ. Sci. Technol.*, 37, 993-1001, [10.1021/es020622f](https://doi.org/10.1021/es020622f), 2003.

698 Shetty, N. J., Pandey, A., Baker, S., Hao, W. M., and Chakrabarty, R. K.: Measuring light absorption by  
699 freshly emitted organic aerosols: Optical artifacts in traditional solvent-extraction-based methods,  
700 *Atmos. Chem. Phys.*, 19, 8817-8830, [10.5194/acp-19-8817-2019](https://doi.org/10.5194/acp-19-8817-2019), 2019.

701 Simoneit, B. R. T., and Fetzer, J. C.: High molecular weight polycyclic aromatic hydrocarbons in  
702 hydrothermal petroleum from the Gulf of California and Northeast Pacific Ocean, *Org. Geochem.*,  
703 24, 1065-1077, [https://doi.org/10.1016/S0146-6380\(96\)00081-2](https://doi.org/10.1016/S0146-6380(96)00081-2), 1996.

704 Simoneit, B. R. T., Elias, V. O., Kobayashi, M., Kawamura, K., Rushdi, A. I., Medeiros, P. M., Rogge,  
705 W. F., and Didyk, B. M.: Sugars dominant water-soluble organic compounds in soils and  
706 characterization as tracers in atmospheric particulate matter, *Environ. Sci. Technol.*, 38, 5939-5949,  
707 [10.1021/es0403099](https://doi.org/10.1021/es0403099), 2004.

708 Song, C., Gyawali, M., Zaveri, R. A., Shilling, J. E., and Arnott, W. P.: Light absorption by secondary  
709 organic aerosol from  $\alpha$ -pinene: Effects of oxidants, seed aerosol acidity, and relative humidity, *J.*  
710 *Geophys. Res. Atmos.*, 118, 11,741-711,749, [10.1002/jgrd.50767](https://doi.org/10.1002/jgrd.50767), 2013.

711 Taylor, N. F., Collins, D. R., Lowenthal, D. H., McCubbin, I. B., Hallar, A. G., Samburova, V., Zielinska,  
712 B., Kumar, N., and Mazzoleni, L. R.: Hygroscopic growth of water soluble organic carbon isolated  
713 from atmospheric aerosol collected at US national parks and Storm Peak Laboratory, *Atmos. Chem.*  
714 *Phys.*, 17, 2555-2571, [10.5194/acp-17-2555-2017](https://doi.org/10.5194/acp-17-2555-2017), 2017.

715 Teich, M., van Pinxteren, D., Wang, M., Kecorius, S., Wang, Z., Müller, T., Močnik, G., and Herrmann,  
716 H.: Contributions of nitrated aromatic compounds to the light absorption of water-soluble and  
717 particulate brown carbon in different atmospheric environments in Germany and China, *Atmos.*  
718 *Chem. Phys.*, 17, 1653-1672, [10.5194/acp-17-1653-2017](https://doi.org/10.5194/acp-17-1653-2017), 2017.

719 Updyke, K. M., Nguyen, T. B., and Nizkorodov, S. A.: Formation of brown carbon via reactions of  
720 ammonia with secondary organic aerosols from biogenic and anthropogenic precursors, *Atmos.*  
721 *Environ.*, 63, 22-31, <https://doi.org/10.1016/j.atmosenv.2012.09.012>, 2012.

722 Wang, X., Heald, C. L., Ridley, D. A., Schwarz, J. P., Spackman, J. R., Perring, A. E., Coe, H., Liu, D.,  
723 and Clarke, A. D.: Exploiting simultaneous observational constraints on mass and absorption to  
724 estimate the global direct radiative forcing of black carbon and brown carbon, *Atmos. Chem. Phys.*,  
725 14, 10989-11010, [10.5194/acp-14-10989-2014](https://doi.org/10.5194/acp-14-10989-2014), 2014.

726 Wang, X., Heald, C. L., Liu, J., Weber, R. J., Campuzano-Jost, P., Jimenez, J. L., Schwarz, J. P., and  
727 Perring, A. E.: Exploring the observational constraints on the simulation of brown carbon, *Atmos.*  
728 *Chem. Phys.*, 18, 635-653, [10.5194/acp-18-635-2018](https://doi.org/10.5194/acp-18-635-2018), 2018.

729 Wang, Y., Hu, M., Wang, Y., Zheng, J., Shang, D., Yang, Y., Liu, Y., Li, X., Tang, R., Zhu, W., Du, Z.,  
730 Wu, Y., Guo, S., Wu, Z., Lou, S., Hallquist, M., and Yu, J. Z.: The formation of nitro-aromatic  
731 compounds under high NO<sub>x</sub> and anthropogenic VOC conditions in urban Beijing, China, *Atmos.*  
732 *Chem. Phys.*, 19, 7649-7665, [10.5194/acp-19-7649-2019](https://doi.org/10.5194/acp-19-7649-2019), 2019.

733 Washenfelder, R. A., Attwood, A. R., Brock, C. A., Guo, H., Xu, L., Weber, R. J., Ng, N. L., Allen, H.  
734 M., Ayres, B. R., Baumann, K., Cohen, R. C., Draper, D. C., Duffey, K. C., Edgerton, E., Fry, J. L.,  
735 Hu, W. W., Jimenez, J. L., Palm, B. B., Romer, P., Stone, E. A., Wooldridge, P. J., and Brown, S. S.:  
736 Biomass burning dominates brown carbon absorption in the rural southeastern United States,  
737 *Geophys. Res. Lett.*, 42, 653-664, [10.1002/2014gl062444](https://doi.org/10.1002/2014gl062444), 2015.

738 Weber, R. J., Sullivan, A. P., Peltier, R. E., Russell, A., Yan, B., Zheng, M., de Gouw, J., Warneke, C.,  
739 Brock, C., Holloway, J. S., Atlas, E. L., and Edgerton, E.: A study of secondary organic aerosol  
740 formation in the anthropogenic-influenced southeastern United States, *J. Geophys. Res. Atmos.*, 112,  
741 D13302, [10.1029/2007jd008408](https://doi.org/10.1029/2007jd008408), 2007.

742 Xie, M., Chen, X., Hays, M. D., Lewandowski, M., Offenberger, J., Kleindienst, T. E., and Holder, A. L.:  
743 Light absorption of secondary organic aerosol: Composition and contribution of nitroaromatic  
744 compounds, *Environ. Sci. Technol.*, 51, 11607-11616, [10.1021/acs.est.7b03263](https://doi.org/10.1021/acs.est.7b03263), 2017a.

745 Xie, M., Hays, M. D., and Holder, A. L.: Light-absorbing organic carbon from prescribed and laboratory

746 biomass burning and gasoline vehicle emissions, *Sci. Rep.*, 7, 7318, 10.1038/s41598-017-06981-8,  
747 2017b.

748 Xie, M., Shen, G., Holder, A. L., Hays, M. D., and Jetter, J. J.: Light absorption of organic carbon emitted  
749 from burning wood, charcoal, and kerosene in household cookstoves, *Environ. Pollut.*, 240, 60-67,  
750 <https://doi.org/10.1016/j.envpol.2018.04.085>, 2018.

751 Xie, M., Chen, X., Hays, M. D., and Holder, A. L.: Composition and light absorption of N-containing  
752 aromatic compounds in organic aerosols from laboratory biomass burning, *Atmos. Chem. Phys.*, 19,  
753 2899-2915, 10.5194/acp-19-2899-2019, 2019a.

754 Xie, M., Chen, X., Holder, A. L., Hays, M. D., Lewandowski, M., Offenber, J. H., Kleindienst, T. E.,  
755 Jaoui, M., and Hannigan, M. P.: Light absorption of organic carbon and its sources at a southeastern  
756 U.S. location in summer, *Environ. Pollut.*, 244, 38-46, <https://doi.org/10.1016/j.envpol.2018.09.125>,  
757 2019b.

758 Xie, M., Zhao, Z., Holder, A. L., Hays, M. D., Chen, X., Shen, G., Jetter, J. J., Champion, W. M., and  
759 Wang, Q.: Chemical composition, structures, and light absorption of N-containing aromatic  
760 compounds emitted from burning wood and charcoal in household cookstoves, *Atmos. Chem. Phys.*,  
761 20, 14077-14090, 10.5194/acp-20-14077-2020, 2020.

762 Xie, M., Peng, X., Shang, Y., Yang, L., Zhang, Y., Wang, Y., and Liao, H.: Collocated measurements of  
763 Light-absorbing organic carbon in PM<sub>2.5</sub>: Observation uncertainty and organic tracer-based source  
764 apportionment, *J. Geophys. Res. Atmos.*, 127, e2021JD035874,  
765 <https://doi.org/10.1029/2021JD035874>, 2022.

766 Xu, Z., Feng, W., Wang, Y., Ye, H., Wang, Y., Liao, H., and Xie, M.: Replication Data for:  
767 Underestimation of brown carbon absorption based on the methanol extraction method and its  
768 impacts on source analysis, Harvard Dataverse, V2, <https://doi.org/10.7910/DVN/CGHPXB>, 2022.

769 Xu, L., Peng, Y., Ram, K., Zhang, Y., Bao, M., and Wei, J.: Investigation of the uncertainties of simulated  
770 optical properties of brown carbon at two Asian sites using a modified bulk aerosol optical scheme  
771 of the community atmospheric model version 5.3, *J. Geophys. Res. Atmos.*, 126, e2020JD033942,  
772 <https://doi.org/10.1029/2020JD033942>, 2021.

773 Yan, F., Kang, S., Sillanpää, M., Hu, Z., Gao, S., Chen, P., Gautam, S., Reinikainen, S.-P., and Li, C.: A  
774 new method for extraction of methanol-soluble brown carbon: Implications for investigation of its  
775 light absorption ability, *Environ. Pollut.*, 262, 114300, <https://doi.org/10.1016/j.envpol.2020.114300>,  
776 2020.

777 Yang, L., Shang, Y., Hannigan, M. P., Zhu, R., Wang, Q. g., Qin, C., and Xie, M.: Collocated speciation  
778 of PM<sub>2.5</sub> using tandem quartz filters in northern nanjing, China: Sampling artifacts and  
779 measurement uncertainty, *Atmos. Environ.*, 246, 118066,  
780 <https://doi.org/10.1016/j.atmosenv.2020.118066>, 2021.

781 Yu, Y., Ding, F., Mu, Y., Xie, M., and Wang, Q. g.: High time-resolved PM<sub>2.5</sub> composition and sources  
782 at an urban site in Yangtze River Delta, China after the implementation of the APPCAP,  
783 *Chemosphere*, 261, 127746, <https://doi.org/10.1016/j.chemosphere.2020.127746>, 2020.

784 Zhang, A., Wang, Y., Zhang, Y., Weber, R. J., Song, Y., Ke, Z., and Zou, Y.: Modeling the global radiative  
785 effect of brown carbon: a potentially larger heating source in the tropical free troposphere than black  
786 carbon, *Atmos. Chem. Phys.*, 20, 1901-1920, 10.5194/acp-20-1901-2020, 2020.

787 Zhang, X., Hecobian, A., Zheng, M., Frank, N. H., and Weber, R. J.: Biomass burning impact on PM<sub>2.5</sub>  
788 over the southeastern US during 2007: integrating chemically speciated FRM filter measurements,  
789 MODIS fire counts and PMF analysis, *Atmos. Chem. Phys.*, 10, 6839-6853, 10.5194/acp-10-6839-  
790 2010, 2010.

791 Zhang, X., Lin, Y.-H., Surratt, J. D., and Weber, R. J.: Sources, composition and absorption Ångström  
792 exponent of light-absorbing organic components in aerosol extracts from the Los Angeles basin,  
793 *Environ. Sci. Technol.*, 47, 3685-3693, 10.1021/es305047b, 2013.

794 Zhu, C.-S., Cao, J.-J., Huang, R.-J., Shen, Z.-X., Wang, Q.-Y., and Zhang, N.-N.: Light absorption  
795 properties of brown carbon over the southeastern Tibetan Plateau, *Sci. Total Environ.*, 625, 246-251,  
796 <https://doi.org/10.1016/j.scitotenv.2017.12.183>, 2018.

Table 1. SEOC concentrations and extraction efficiencies ( $\eta$ , %) of total OC and OC fractions for different solvents.

	OC prior to extractions	Water <sup>a</sup>	MeOH <sup>b</sup>	MeOH/DCM (1:1) <sup>b</sup>	MeOH/DCM (1:2) <sup>b</sup>	THF <sup>b</sup>	DMF <sup>a</sup>
<b>One-time extraction (N = 11)</b>							
<i>SEOC, <math>\mu\text{g m}^{-3}</math></i>							
Total OC	9.36 ± 2.27	6.38 ± 2.03	7.85 ± 2.40	7.08 ± 1.32	6.99 ± 1.71	6.14 ± 2.01	8.49 ± 2.52
OC1	0.66 ± 0.21	0.61 ± 0.20	0.64 ± 0.21	0.65 ± 0.20	0.64 ± 0.22	0.59 ± 0.18	0.59 ± 0.24
OC2	2.69 ± 0.55	2.20 ± 0.60	2.50 ± 0.55	2.34 ± 0.41	2.37 ± 0.46	2.09 ± 0.55	2.48 ± 0.60
OC3	3.35 ± 0.93	1.82 ± 0.80	2.48 ± 0.96	2.23 ± 0.49	2.18 ± 0.70	1.98 ± 0.93	2.86 ± 1.01
OC4	2.75 ± 0.81	1.76 ± 0.65	2.23 ± 0.84	1.86 ± 0.51	1.78 ± 0.61	1.48 ± 0.61	2.56 ± 0.87
<i><math>\eta</math> (%)</i>							
Total OC		66.7 ± 8.58	82.3 ± 8.68	76.0 ± 7.70	74.3 ± 7.83	64.2 ± 8.08	89.0 ± 7.96
OC1		91.7 ± 4.85	96.1 ± 6.73	97.9 ± 5.02	97.4 ± 4.35	89.6 ± 9.55	88.8 ± 4.98
OC2		80.8 ± 8.11	92.7 ± 3.69	87.7 ± 5.87	88.5 ± 7.21	76.9 ± 7.62	91.4 ± 6.17
OC3		52.4 ± 11.8	73.0 ± 11.5	68.1 ± 8.64	65.2 ± 10.2	57.6 ± 12.0	84.3 ± 9.79
OC4		63.3 ± 9.13	80.3 ± 11.4	69.0 ± 9.26	64.5 ± 8.11	52.7 ± 5.86	92.8 ± 9.69
<b>Two-time extraction (N = 10)</b>							
<i>SEOC, <math>\mu\text{g m}^{-3}</math></i>							
Total OC	10.9 ± 4.93	7.74 ± 4.01	9.33 ± 4.11	9.34 ± 4.19	9.11 ± 4.04	7.56 ± 3.38	10.4 ± 4.80
OC1	0.66 ± 0.47	0.62 ± 0.45	0.62 ± 0.49	0.59 ± 0.50	0.60 ± 0.51	0.59 ± 0.49	0.60 ± 0.47
OC2	2.76 ± 0.77	2.20 ± 0.59	2.60 ± 0.66	2.57 ± 0.65	2.60 ± 0.68	2.28 ± 0.53	2.69 ± 0.78
OC3	4.11 ± 2.01	2.55 ± 1.62	3.26 ± 1.62	3.37 ± 1.68	3.20 ± 1.58	2.62 ± 1.39	3.88 ± 1.95
OC4	3.36 ± 1.77	2.38 ± 1.42	2.84 ± 1.42	2.81 ± 1.47	2.71 ± 1.39	2.08 ± 1.06	3.23 ± 1.70
<i><math>\eta</math> (%)</i>							
Total OC		69.9 ± 5.88	86.6 ± 7.86	86.2 ± 8.73	84.8 ± 7.76	70.1 ± 8.01	95.6 ± 3.67
OC1		93.6 ± 4.08	90.3 ± 13.9	82.6 ± 25.9	83.8 ± 22.4	82.9 ± 15.1	92.2 ± 13.9
OC2		80.1 ± 5.01	94.8 ± 4.20	93.6 ± 4.94	94.7 ± 2.51	83.5 ± 6.86	97.2 ± 2.12
OC3		59.0 ± 10.6	80.0 ± 10.2	82.3 ± 9.86	79.1 ± 10.6	63.9 ± 10.7	94.2 ± 4.15
OC4		69.3 ± 6.46	86.3 ± 12.0	84.3 ± 12.0	82.7 ± 13.3	62.9 ± 7.76	96.9 ± 5.18

<sup>a</sup> Concentrations of rOC in extracted filters were measured after the baking process (100 °C, 2 h); <sup>b</sup> rOC was measured when extracted filters were air dried.

Table 2. Light-absorbing properties of SEOC following one-time and two-time extraction procedures.

Solvent	Water	MeOH	MeOH/DCM (1:1)	MeOH/DCM (1:2)	THF	DMF
<b>One-time extraction</b>						
Abs <sub>365</sub> , Mm <sup>-1</sup>	5.13 ± 2.04	11.9 ± 5.83	10.3 ± 4.42	8.12 ± 3.38	5.48 ± 3.01	17.5 ± 8.05
Abs <sub>550</sub> , Mm <sup>-1</sup>	0.35 ± 0.12	1.28 ± 0.87	0.97 ± 0.55	0.35 ± 0.47	0.42 ± 0.47	4.40 ± 2.34
MAE <sub>365</sub> , m <sup>2</sup> g <sup>-1</sup> C	0.87 ± 0.19	1.46 ± 0.41	1.41 ± 0.36	1.13 ± 0.22	0.87 ± 0.25	2.02 ± 0.58
MAE <sub>550</sub> , m <sup>2</sup> g <sup>-1</sup> C	0.062 ± 0.028	0.15 ± 0.084	0.13 ± 0.054	0.042 ± 0.52	0.059 ± 0.56	0.30 ± 0.12
Å	6.63 ± 0.49	5.44 ± 0.75	5.65 ± 0.54	6.59 ± 0.66	6.17 ± 0.69	4.52 ± 0.41
<b>Two-time extraction</b>						
Abs <sub>365,1st</sub> , <sup>a</sup> Mm <sup>-1</sup>	6.64 ± 4.25	14.1 ± 7.09	14.6 ± 8.05	11.6 ± 6.78	7.17 ± 4.26	20.5 ± 10.6
Abs <sub>550,1st</sub> , <sup>a</sup> Mm <sup>-1</sup>	0.42 ± 0.12	1.34 ± 0.70	1.34 ± 0.83	0.84 ± 0.50	0.53 ± 0.27	2.82 ± 1.44
Abs <sub>365</sub> , <sup>b</sup> Mm <sup>-1</sup>	8.26 ± 5.21	15.5 ± 7.76	16.8 ± 8.82	14.0 ± 8.91	8.35 ± 4.81	21.9 ± 11.2
Abs <sub>550</sub> , <sup>b</sup> Mm <sup>-1</sup>	0.50 ± 0.18	1.60 ± 0.78	1.64 ± 0.99	1.22 ± 0.98	0.69 ± 0.43	3.01 ± 1.49
MAE <sub>365</sub> , m <sup>2</sup> g <sup>-1</sup> C	1.19 ± 0.26	1.70 ± 0.60	1.80 ± 0.52	1.50 ± 0.51	1.10 ± 0.40	2.11 ± 0.49
MAE <sub>550</sub> , m <sup>2</sup> g <sup>-1</sup> C	0.082 ± 0.30	0.19 ± 0.11	0.17 ± 0.083	0.13 ± 0.069	0.094 ± 0.054	0.29 ± 0.075
Å	6.32 ± 0.58	5.37 ± 0.57	5.47 ± 0.67	5.57 ± 0.39	6.06 ± 0.54	4.53 ± 0.21

<sup>a</sup> Light absorption coefficient of SEOC after the first extraction; <sup>b</sup> sum of SEOC absorption in 1<sup>st</sup> and 2<sup>nd</sup> extracts.

Table 3. Comparisons of light-absorbing properties of ambient PM<sub>2.5</sub> extracts in DMF and MeOH derived from duplicate Q<sub>f</sub>-Q<sub>b</sub> data (*N* = 109).

	DMF			MeOH <sup>a</sup>		
	Median	Mean ± std	Range	Median	Mean ± std	Range
Abs <sub>365</sub> , Mm <sup>-1</sup>	6.99	8.42 ± 5.40	1.14–30.8	5.59	6.43 ± 4.66	0.38–29.6
MAE <sub>365</sub> , m <sup>2</sup> g <sup>-1</sup> C	1.13	1.20 ± 0.49	0.34–2.45	0.91	1.03 ± 0.58	0.089–2.49
Å	5.21	5.25 ± 0.64	3.21–6.82	6.49	6.81 ± 1.64	4.34–11.3

<sup>a</sup> Data for MeOH extracts were obtained from Xie et al. (2022).

Figure 1

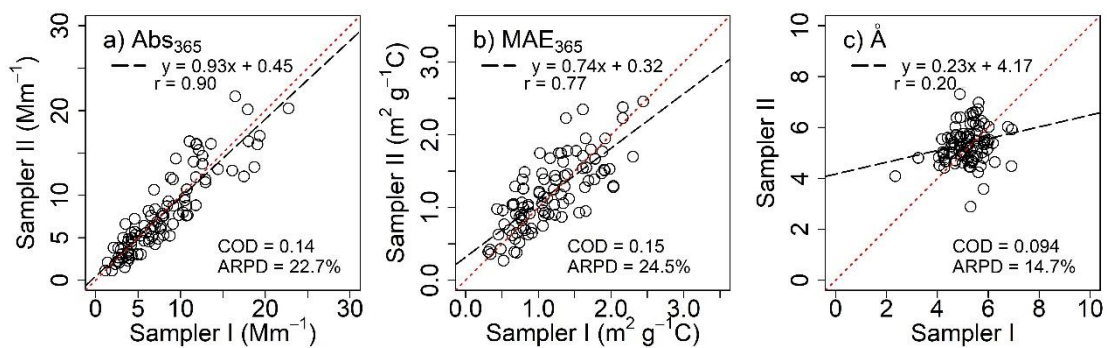


Figure 1. Comparisons between collocated measurements for light-absorbing properties of  $PM_{2.5}$  extracts in DMF after  $Q_b$  corrections.

Figure 2

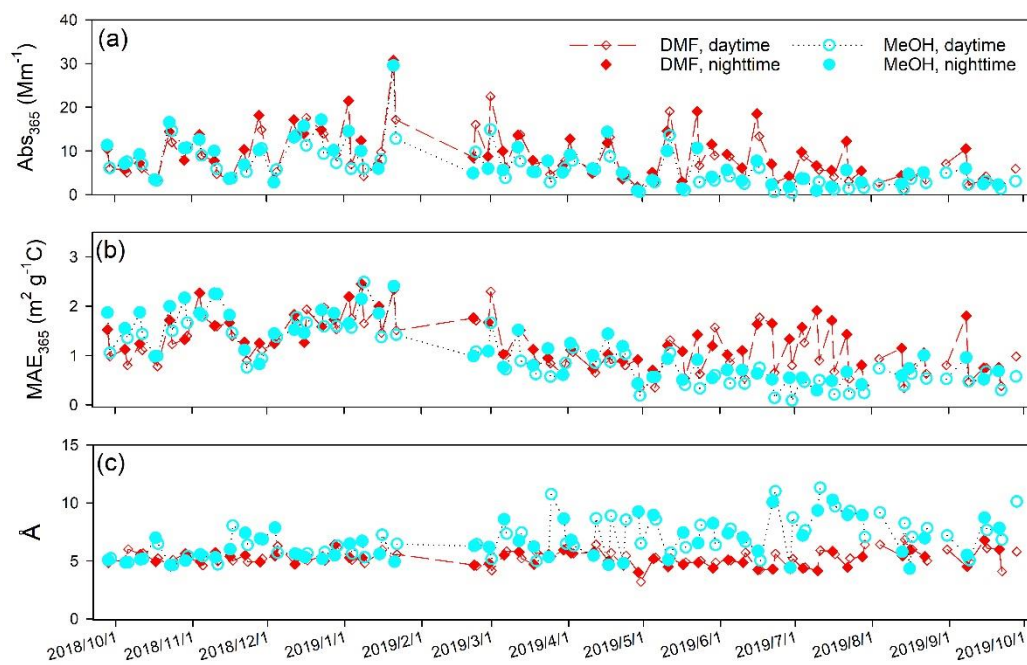


Figure 2. Time series comparisons of light-absorbing properties of DMF and MeOH extracts using artifact-corrected data. MeOH extract data were obtained from Xie et al. (2022).

Figure 3

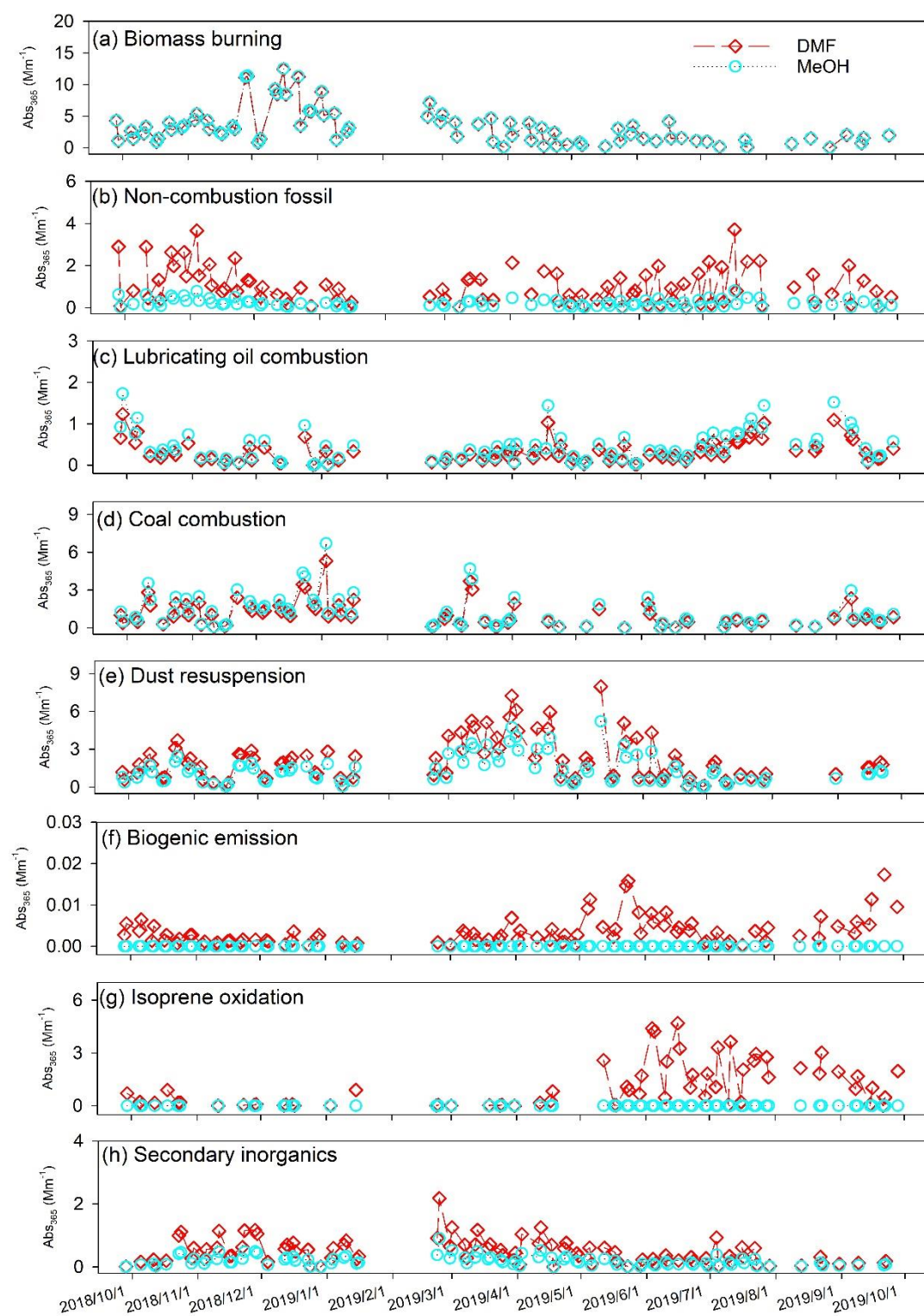


Figure 3. Time series of factor contributions to  $Abs_{365}$  of DMF and MeOH extracts of ambient PM<sub>2.5</sub> samples.